Nanoscale

COMMUNICATION

View Article Online
View Journal | View Issue

Cite this: *Nanoscale*, 2023, **15**, 109

Received 22nd September 2022,
Accepted 21st November 2022

DOI: 10.1039/d2nr05225c

rsc.li/nanoscale

Structure and assembly of a hexanuclear AuNi bimetallic nanocluster†

Cheng-Bo Tao, Ji-Qiang Fan, Wenwen Fei, Yan Zhao* and Man-Bo Li *

An Au_4Ni_2 nanocluster containing a square-planar [$-PPh_2-Au-S-Au-]_2$ ring and two nickel-pincer arms is reported here. Abundant intra- and inter-cluster noncovalent interactions promote the assembly of the nanocluster into a porous framework material. The assembly-dependent unique solubility and photoluminescence were also investigated.

Institute of Physical Science and Information Technology, Key Laboratory of Structure and Functional Regulation of Hybrid Materials of Ministry of Education, Anhui University, Hefei 230601, P.R. China. E-mail: 20231@ahu.edu.cn, mbli@ahu.edu.cn

†Electronic supplementary information (ESI) available. CCDC 2208033 and 2208034. For ESI and crystallographic data in CIF or other electronic format see DOI: https://doi.org/10.1039/d2nr05225c

Man-Bo Li

Man-Bo Li was born in Hubei, China in 1986. He received his B.S. (2008) and Ph.D (2013) degrees from the University of Science and Technology of China under the supervision of Prof. Shi-Kai Tian. After three years of research work on metal nanoclusters with Prof. Zhikun Wu at the Hefei Institutes of Physical Science, Chinese Academy of Sciences and a short stay at King Abdullah University of Science and Technology for research on heterogeneous catalysis, he joined Prof. Jan-E. Bäckvall's research group at Stockholm University to develop palladium nanocluster-catalyzed oxidative reactions (2017–2019). In December 2019, he started his independent academic career as a professor at Anhui University, China. His current research interests focus on the construction of atomically precise nanoclusters and the discovery of their catalytic performance.

The emerging molecule-like metal nanoclusters[1–7] are composed of a metal framework and surface ligands with an atomically precise composition and structure. Both their size and structure bridge the gap of organometallic complexes and metal nanoparticles, often triggering unique properties[8–14] different from the latter two metal species. Meanwhile, the precise structure of the metal nanoclusters enables an in-depth investigation of the structure–property correlation at the atomic level.[15–17] Thus, the discovery of metal nanoclusters with unique frameworks and bonding structures constitutes an important part of the research in this area. Since the pioneering works on the structural determination of $Au_{102}(SC_6H_4COOH)_{44}$ [18] and $Au_{25}(SC_2H_4Ph)_{18}$,[19,20] hundreds of metal nanoclusters' crystal structures have been reported. Among them, structural units such as the 13-metal-atom icosahedron (M_{13}),[21–23] the 8-metal-atom cube (M_8),[24–26] and the 4-metal-atom tetrahedron (M_4)[27–29] are not only stable cluster forms, but also building blocks in hierarchically structured nanoclusters.

The 6-metal-atom nanocluster (M_6) was first represented by the copper hydride $(HCuPPh_3)_6$ in 1971,[30] demonstrating an octahedral geometry. After that, octahedral M_6 nanoclusters protected by thiolate,[31] phosphine[32,33] and N-heterocyclic carbene[34] were successively synthesized. Despite the reports on M_6 nanoclusters with other geometries, such as edge-sharing bitetrahedral Au_6 [35] and tiara-like Ni_6,[36] the octahedral arrangement of metal atoms in M_6-based systems is dominant. In particular, two vertexes doped octahedral Au_4M_2 nanoclusters such as Au_4Pt_2, Au_4Pd_2, and Au_4Ni_2 showed the doping effect, demonstrating attractive performance, such as high activity in electrochemical nitrogen reduction.[37,38] Based on the previous reports, two interesting questions arise: (i) can we break the preferred octahedral arrangement of the Au_4M_2 system to achieve novel structures? (ii) How does the novel Au_4M_2 structure impact its properties? Inspired by the previous works on controlling the atomically precise structure of metal nanoclusters by regulating the electronic and steric effects of ligands,[39–41] herein, we obtained a new Au_4Ni_2 nano-

cluster by introducing pincer complexes in the synthesis of nanoclusters. This novel Au_4Ni_2 consists of a square-planar $[-PPh_2-Au-S-Au-]_2$ ring and two nickel-pincer arms, featuring abundant inter- and intra-cluster noncovalent interactions. The assembly of Au_4Ni_2 molecules into a porous framework material was revealed and the assembly-related intriguing properties were also shown.

An attempt to synthesize structurally different AuNi bimetallic nanoclusters from the conventional octahedral Au_4M_2 nanocluster was initiated by the use of two pincer complexes: pyridine-2,6-diyldimethanethiol (SNS, **1**)[42] and NiCl[(1,3-bis ((diphenylphosphanyl)oxy)benzene] (NiCl-PCP, **2**).[43] Pincer complexes were first introduced by Shaw and van Koten in the late 1970s.[44,45] They are generally tri-coordinated ligands featuring a central aromatic ring that is *ortho–ortho*-disubstituted with two electron-donor substituents.[46] We envisioned that the introduction of rigid pincer complexes would break the conventional arrangement of metal atoms in metal nanoclusters, triggering the formation of nanoclusters with unique structures. After screening different solvents and reductants, an optimized reaction procedure afforded a yellow-colored reaction system, which was purified by column chromatography or recrystallization to obtain the nanocluster product (**3**) in satisfactory yield (Fig. 1a, for details, see the ESI,† p. S4). The UV-vis spectrum of **3** in dichloromethane showed three absorption bands centered at 350, 380 and 430 nm (Fig. S3a†). The similar profiles (Fig. S3b†) of the FT-IR spectra of **3** and **2** suggest that the structural unit of NiCl-PCP is retained in the nanocluster. MALDI-TOF-MS gave a single peak of the nanocluster at 2294.07 Da (Fig. S4†), indicating that the composition of **3** is probably $Au_4Ni_2(PPh_2)_2S_2(PCP)_2$.

Crystallization of **3** in the mixed solvents of dichloromethane and pentane gave cubic crystals, which were suitable for structural determination by single-crystal X-ray diffraction (SC-XRD). From the total structure (Fig. 1a, for details, see Fig. S5†), **3** is composed of a hexanuclear Au_4Ni_2, two PPh_2 groups, two S atoms, and two PCP pincer complexes. The resulted molecular fomula is consistent with that revealed by MALDI-TOF-MS. The structure of Au_4Ni_2 (**3**) suggests a $C(sp^3)$–S bond cleavage of **1** during the cluster formation process (Fig. 1a), offering two sulfur atoms. In the meantime, **2** participates in the cluster formation from two aspects. On the one hand, a similar cleavage of the O–P bond offers PPh_2 groups. On the other hand, a Cl dissociation and a subsequent S association occur, generating the two nickel-pincer arms located at the two sulfur sites of Au_4Ni_2 (**3**). Considering that the SNS pincer complex **1** only contributes sulfur atoms, we tried to replace it by other sulfur sources that were commonly applied in the preparation of metal nanoclusters, such as thiophenols and thioalcohols (RSH) (for details, see the ESI,† p. S4). However, these attampts failed to give Au_4Ni_2 (**3**), instead NiSR-PCP complexes were obtained as the major products (Fig. S1†). As a typical example, the replacement of **1** by 4-*tert*-butylthiophenol (TBBT) under the standard reaction conditions gave NiTBBT-PCP (**4**, for its structural determination by SC-XRD, see Fig. S2†) instead of the AuNi bimetallic nanocluster Au_4Ni_2 (**3**). These control experiments indicate that the SNS pincer complex **1** is crucial for the formation of Au_4Ni_2 (**3**). A reasonable explanation might be that the rigid **1** circumvents its bonding to sterically hindered **2**, thus proceeding with $C(sp^3)$–S bond cleavage instead to give Au_4Ni_2 (**3**).

The framework of Au_4Ni_2 (**3**) is different from the previously reported octahedral Au_4M_2 system. Taking $Au_4Ni_2(SPhMe_2)_8$[38] as an example, its four Au and two Ni atoms form a distorted octahedral structure, which is further capped by the eight –SR groups existing at the vertex of the Au–Ni kernel (Fig. 1e).

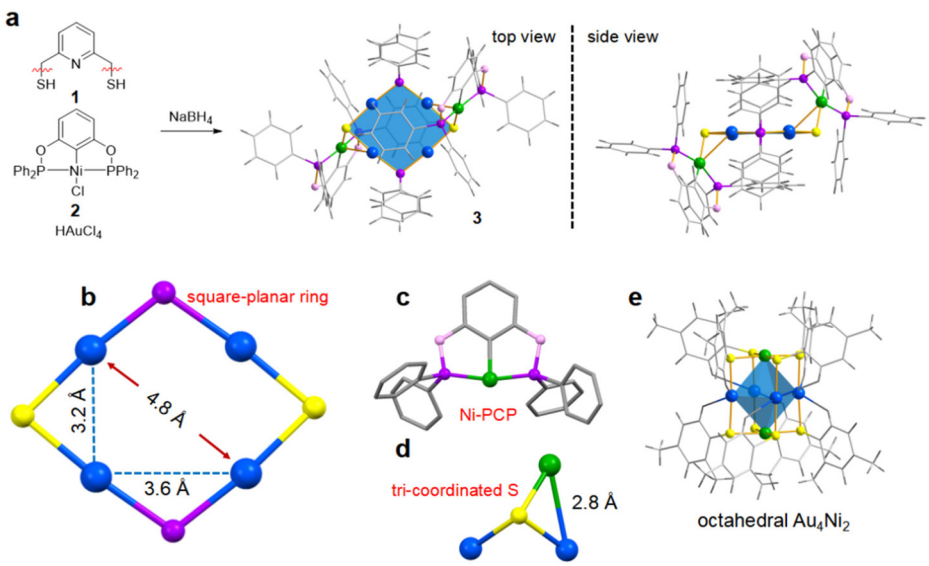

Fig. 1 (a) Synthesis and total structure of Au_4Ni_2 (**3**); (b–d) structural anatomy of Au_4Ni_2 (**3**); (e) structure of Au_4Ni_2 (octahedral). Blue: Au; green: Ni; purple: P; pink: O; yellow: S; gray: C and H.

Comparatively, in Au_4Ni_2 (**3**), both the S and P atoms are in a plane with the four Au atoms, forming a square-planar $[-PPh_2-Au-S-Au-]_2$ ring. Two Ni-PCP arms are located at the S sites. The structural features of Au_4Ni_2 (**3**) can be highlighted as follows: (1) four Au atoms, two P atoms and two S atoms form a square-planar ring (Fig. 1b). With the participation of P and S atoms in the Au_4 plane, the average distances of the adjacent gold atoms and the opposite gold atoms are respectively 3.4 and 4.8 Å, which are longer than those in octahedral M_6 systems.[30–38] The open and giant $[-PPh_2-Au-S-Au-]_2$ ring would be a potential site for further applications such as catalysis and molecular recognition. (2) The rigid Ni-PCP pincer complex was introduced in nanoclusters for the first time (Fig. 1c). The two nickel-pincer arms including fourteen rings highly enrich the noncovalent C–H···π and H···H interactions as well as the rigidity of the nanocluster. (3) The S atoms in Au_4Ni_2 (**3**) tri-coordinate to three metal atoms (two Au atoms and one Ni atom), which is distinct from the common di-coordination way in the reported thiolate metal nanoclusters.[47] The lengths of Ni–S and Au–S bonds are similar to be 2.2, 2.3 and 2.3 Å, respectively. The Ni atom is close to one of Au atoms to form a 2.8 Å of Au–Ni bond (Fig. 1d). The unique coordination mode results in two "naked" S atoms which are not bonding to any organic species.

The alternate array of aromatic rings in Au_4Ni_2 (**3**) crystals leads to abundant intra- and inter-cluster noncovalent interactions. Representative intra-cluster interactions are shown in Fig. 2a (also see Fig. S6 and Table S1†). The H···H interactions (marked with red) are mainly attributed to the close distances (2.6 and 2.8 Å) of the phenyl groups on the Ni-PCP arm and the $[-PPh_2-Au-S-Au-]_2$ plane. The C–H···π interactions (marked with cyan) mainly originate from the rigid Ni-PCP pincer arms, including the C–H···π distance of 3.2 Å inside Ni-PCP, and the C–H···π distances of 2.9 and 3.2 Å between the Ni-PCP pincer arms and the $[-PPh_2-Au-S-Au-]_2$ plane. The inter-cluster C–H···π and H···H interactions can be divided into two types. As shown in Fig. 2b (also see Fig. S7–S9 and Tables S2–S4†), the interactions along the *y* axis, including the C–H···π distances (marked with cyan) ranging from 3.2 to 3.5 Å and the H···H distances (marked with red) ranging from 2.7 to 2.9 Å, are attributed to the close distances between the benzene rings on the Ni-PCP arm of one Au_4Ni_2 (**3**) molecule and the PPh_2 groups on the $[-PPh_2-Au-S-Au-]_2$ plane of the adjacent Au_4Ni_2 (**3**) molecule. The interactions along the *z* axis mainly originate from the aromatic rings of the rigid Ni-PCP arms that belong to two adjacent Au_4Ni_2 (**3**) molecules. Based on the observations, we found that the abundant inter-cluster noncovalent interactions induce the assembly of the nanocluster molecules into a porous framework material. The pore size on the *yz* surface was approximately 13.9 Å × 8.1 Å, thus generating rectangular channels along the *x* axis. Apart from this kind of channel, two other smaller channels with sizes of 8.3 Å × 3.4 Å and 4.5 Å × 4.1 Å were also observed along the *y* and *z* axes (Fig. S10†).

Owing to the abundant inter-cluster noncovalent interaction-induced assembly of Au_4Ni_2 (**3**) molecules, this nanocluster showed much lower solubility compared with octahedral Au_4Ni_2 (for the determination of the solubility, see Fig. S11–13†). As shown in Fig. 3, the concentrations of the saturated Au_4Ni_2 (octahedral) solutions in commonly used solvents such as dichloromethane (DCM), toluene (Tol), tetrahydrofuran (THF) and ethyl acetate (EA) were 1.6×10^{-2}, 1.5×10^{-2}, 1.4×10^{-2} and 1.0×10^{-2} mol L^{-1}, respectively. In contrast, the concentrations of the saturated solutions of Au_4Ni_2

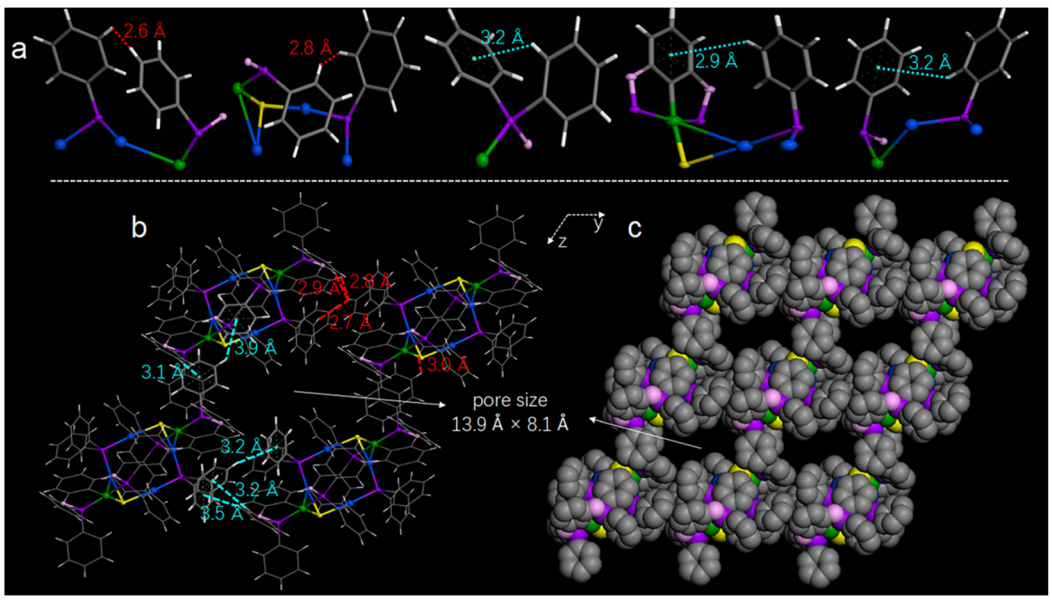

Fig. 2 (a and b) Representative intra- and inter-cluster C–H···π (cyan) and H···H (red) interactions of Au_4Ni_2 (**3**). (c) The cluster-based porous framework material.

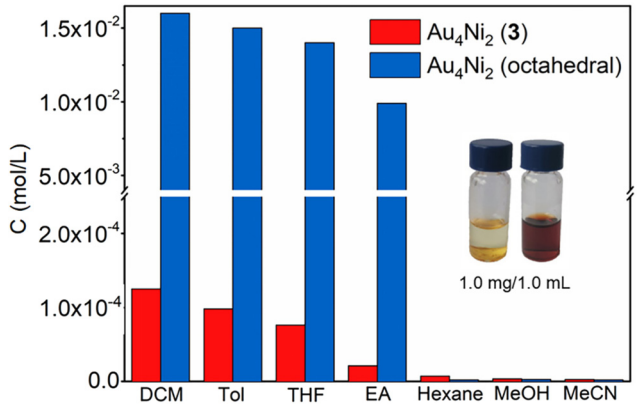

Fig. 3 Comparison of the solubility of Au_4Ni_2 (**3**) and Au_4Ni_2 (octahedral) in different solvents. Inset: the photographs of a system of 1.0 mg of Au_4Ni_2 (**3**) (left) or Au_4Ni_2 (octahedral) (right) in 1.0 mL of DCM.

(**3**) in the four solvents were only 1.2×10^{-4}, 1.0×10^{-4}, 0.8×10^{-4} and 0.2×10^{-4} mol L^{-1}, respectively. These results indicate that the solubility of Au_4Ni_2 (octahedral) is at least 100 times higher (Fig. 3, inset) than that of Au_4Ni_2 (**3**), which could be ascribed to the assembly of Au_4Ni_2 (**3**) into the 3D material. Au_4Ni_2 (**3**) also showed low solubility in other solvents, such as hexane, MeOH and MeCN.

The assembly of Au_4Ni_2 (**3**) also results in its distinct photoluminescence between the crystalline and solution states. As shown in Fig. S14,† the saturated Au_4Ni_2 (**3**) solutions in DCM, Tol, THF and EA showed a similar photoluminescence, while the crystalline Au_4Ni_2 (**3**) showed a different photoluminescence spectrum compared with the dissolved samples, with an improved fluorescence intensity and an approximately 15 nm bathochromic shift of the emissive wavelength (Fig. S14a†). The photoluminescence spectra at different excitation wavelengths (Fig. S14b and c†) further confirmed the intensity increase of the crystalline states of Au_4Ni_2 (**3**). Comparatively, for Au_4Ni_2 (octahedral), its crystalline and solution states exhibited the basically same photoluminescence (Fig. S14d†). The difference in the photoluminescence of crystalline and dissolved Au_4Ni_2 (**3**) is probably ascribed to the assembly restricting the vibration and rotation of nanocluster molecules, thus improving the photoluminescence of Au_4Ni_2 (**3**) in the crystalline state. In the solution state, the large amount of solvent would disturb the noncovalent interactions and thus weaken the nanocluster's luminescence. Au_4Ni_2 (**3**) is ultra-stable, showing the consistent UV-vis spectra in DCM under ambient conditions for one month (Fig. S15a†). Further investigation reveals that it is robust under harsh conditions such as high temperature (Fig. S15b†) and oxidative (Fig. S16a†) and reductive (Fig. S16b†) environments. Its high stability can be explained by the large electrochemical gap (2.22 V) and the relatively high oxidation (1.27 V) and reduction (−0.95 V) barriers that were evaluated by differential pulse voltammetry (DPV, Fig. S17†). Further stability tests under the oxidative and reductive conditions were conducted with cyclic voltammetry (CV) experiments (Fig. S18†), which indicates that Au_4Ni_2 (**3**) is quite robust and recyclable. The stability and recyclability of the nanocluster under various conditions would be highly valuable for its further applications.

Conclusions

In summary, we successfully synthesized a novel hexanuclear AuNi bimetallic nanocluster using pincer complexes. It is different from the octahedral M_6 system, demonstrating a square-planar $[-PPh_2-Au-S-Au-]_2$ ring and two nickel-pincer arms. Unconventional $C(sp^3)$–S bond and O–P bond cleavage of the pincer complexes were observed during the cluster-formation process. The rigid Ni-PCP pincer arms induce abundant intra- and inter-cluster noncovalent interactions, triggering the self-assembly of the nanocluster into a porous framework material. The assembly results in low solubility and distinct photoluminescence in the crystalline and solution states of the nanocluster. Further studies on the applications of the hexanuclear AuNi bimetallic pincer nanocluster in catalysis and gas separation are underway in our laboratory.

Author contributions

M.-B. L. supervised and guided the research, summarized the data, and wrote the manuscript. C.-B. T. and J.-Q. F. carried out the experiments. W. F. resolved the structure of the metal nanocluster. Y. Z. helped in guiding the research and summarized the data. All authors contributed to the preparation of the manuscript.

Conflicts of interest

There are no conflicts to declare.

Acknowledgements

This work was financially supported by the National Natural Science Foundation of China (92061110), the Anhui Provincial Natural Science Foundation (2108085Y05), and the Hefei National Laboratory for Physical Sciences at the Microscale (KF2020102).

References

1 Y. Li, M. Zhou and R. Jin, *Adv. Mater.*, 2021, **33**, 2006591.
2 J. Yan, B. K. Teo and N. Zheng, *Acc. Chem. Res.*, 2018, **51**, 3084–3093.
3 Y. Lu and W. Chen, *Chem. Soc. Rev.*, 2012, **41**, 3594–3623.
4 Z. Lei, X.-K. Wan, S.-F. Yuan, Z.-J. Guan and Q.-M. Wang, *Acc. Chem. Res.*, 2018, **51**, 2465–2474.

5 N. A. Sakthivel and A. Dass, *Acc. Chem. Res.*, 2018, **51**, 1774–1783.
6 S. Takano, S. Hasegawa, M. Suyama and T. Tsukuda, *Acc. Chem. Res.*, 2018, **51**, 3074–3083.
7 A. Ghosh, O. F. Mohammed and O. M. Bakr, *Acc. Chem. Res.*, 2018, **51**, 3094–3103.
8 Q.-F. Zhang, X. Chen and L.-S. Wang, *Acc. Chem. Res.*, 2018, **51**, 2159–2168.
9 S. Hossain, Y. Niihori, L. V. Nair, B. Kumar, W. Kurashige and Y. Negishi, *Acc. Chem. Res.*, 2018, **51**, 3114–3124.
10 Y. Du, H. Sheng, D. Astruc and M. Zhu, *Chem. Rev.*, 2020, **120**, 526–622.
11 B. Nieto-Ortega and T. Bürgi, *Acc. Chem. Res.*, 2018, **51**, 2811–2819.
12 K. Kwak and D. Lee, *Acc. Chem. Res.*, 2019, **52**, 12–22.
13 M. Agrachev, M. Ruzzi, A. Venzo and F. Maran, *Acc. Chem. Res.*, 2019, **52**, 44–52.
14 D. Yang, Y. Sun, X. Cai, W. Hu, Y. Dai, Y. Zhu and Y. Yang, *CCS Chem.*, 2021, **3**, 2771–2799.
15 C. M. Aikens, *Acc. Chem. Res.*, 2018, **51**, 3065–3073.
16 W. Xu, X. Zeng and Y. Gao, *Acc. Chem. Res.*, 2018, **51**, 2739–2747.
17 Q. Tang, G. Hu, V. Fung and D. Jiang, *Acc. Chem. Res.*, 2018, **51**, 2793–2802.
18 P. D. Jadzinsky, G. Calero, C. J. Ackerson, D. A. Bushnell and R. D. Kornberg, *Science*, 2007, **318**, 430–433.
19 M. Zhu, C. M. Aikens, F. J. Hollander, G. C. Schatz and R. Jin, *J. Am. Chem. Soc.*, 2008, **130**, 5883–5885.
20 M. W. Heaven, A. Dass, P. S. White, K. M. Holt and R. W. Murray, *J. Am. Chem. Soc.*, 2008, **130**, 3754–3755.
21 M. R. Narouz, S. Takano, P. A. Lummis, T. I. Levchenko, A. Nazemi, S. Kaappa, S. Malola, G. Yousefalizadeh, L. A. Calhoun, K. G. Stamplecoskie, H. Hakkinen, T. Tsukuda and C. M. Crudden, *J. Am. Chem. Soc.*, 2019, **141**, 14997–15002.
22 C. Zhang, Z. Wang, W.-D. Si, L. Wang, J.-M. Dou, Z.-Y. Gao, C.-H. Tung and D. Sun, *ACS Nano*, 2022, **16**, 9598–9607.
23 S. Jin, X. Zou, L. Xiong, W. Du, S. Wang, Y. Pei and M. Zhu, *Angew. Chem., Int. Ed.*, 2018, **57**, 16768–16772.
24 S. Zhang, L. Feng, R. D. Senanayake, C. M. Aikens, X.-P. Wang, Q.-Q. Zhao, C.-H. Tung and D. Sun, *Chem. Sci.*, 2018, **9**, 1251–1258.
25 M.-M. Zhang, X.-Y. Dong, Z.-Y. Wang, H.-Y. Li, S.-J. Li, X. Zhao and S.-Q. Zang, *Angew. Chem., Int. Ed.*, 2020, **59**, 10052–10058.
26 X. Kang, S. Wang, Y. Song, S. Jin, G. Sun, H. Yu and M. Zhu, *Angew. Chem., Int. Ed.*, 2016, **55**, 3611–3614.
27 G. Feng, M. Zhang, D. Shao, X. Wan, S. Wan, L. Maron and C. Zhu, *Nat. Chem.*, 2019, **11**, 248–253.
28 Z. He, Y. Yang, J. Zou, Q. You, L. Feng, M.-B. Li and Z. Wu, *Chem. – Eur. J.*, 2022, **28**, e202200212.
29 A. W. Cook, Z. R. Jones, G. Wu, S. L. Scott and T. W. Hayton, *J. Am. Chem. Soc.*, 2018, **140**, 394–400.
30 T. Richerzhagen and D. H. Volman, *J. Am. Chem. Soc.*, 1971, 2063–2065.
31 Z. Han, X.-Y. Dong, P. Luo, S. Li, Z.-Y. Wang, S.-Q. Zang and T. C. W. Mak, *Sci. Adv.*, 2020, **6**, eaay0107.
32 M. A. Bakar, M. Sugiuchi, M. Iwasaki, Y. Shichibu and K. Konishi, *Nat. Commun.*, 2017, **8**, 576.
33 E. S. Smirnova and A. M. Echavarren, *Angew. Chem., Int. Ed.*, 2013, **52**, 9023–9026.
34 X.-L. Pei, P. Zhao, H. Ube, Z. Lei, K. Nagata, M. Ehara and M. Shionoya, *J. Am. Chem. Soc.*, 2022, **144**, 2156–2163.
35 C. E. Briant, K. P. Hall and D. M. P. Mingos, *J. Organomet. Chem.*, 1983, **254**, 18–20.
36 M. Zhu, S. Zhou, C. Yao, L. Liao and Z. Wu, *Nanoscale*, 2014, **6**, 14195–14199.
37 C. Yao, N. Guo, S. Xi, C. Xu, W. Liu, X. Zhao, J. Li, H. Fang, J. Su, Z. Chen, H. Yan, Z. Qiu, P. Lyu, C. Chen, H. Xu, X. Peng, X. Li, B. Liu, C. Su, S. J. Pennycook, C.-J. Sun, J. Li, C. Zhang, Y. Du and J. Lu, *Nat. Commun.*, 2020, **11**, 4389.
38 M. Han, M. Guo, Y. Yun, Y. Xu, H. Sheng, Y. Chen, Y. Du, K. Ni, Y. Zhu and M. Zhu, *Adv. Funct. Mater.*, 2022, **32**, 2202820.
39 H. Xiang, H. Yan, J. Liu, R. Cheng, C.-Q. Xu, J. Li and C. Yao, *J. Am. Chem. Soc.*, 2022, **144**, 14248–14257.
40 R. W. Y. Man, H. Yi, S. Malola, S. Takano, T. Tsukuda, H. Häkkinen, M. Nambo and C. M. Crudden, *J. Am. Chem. Soc.*, 2022, **144**, 2056–2061.
41 Y. Hua, J.-H. Huang, Z.-H. Shao, X.-M. Luo, Z.-Y. Wang, J.-Q. Liu, X. Zhao, X. Chen and S.-Q. Zang, *Adv. Mater.*, 2022, **34**, 2203734.
42 S. Dey, M. E. Ahmed and A. Dey, *Inorg. Chem.*, 2018, **57**, 5939–5947.
43 B. Vabre, F. Lindeperg and D. Zargarian, *Green Chem.*, 2013, **15**, 3188–3194.
44 C. J. Moulton and B. L. Shaw, *J. Chem. Soc., Dalton Trans.*, 1976, 1020–1024.
45 G. van Koten, K. Timmer, J. G. Nolte and A. L. Spek, *J. Chem. Soc., Chem. Commun.*, 1978, 250–252.
46 E. Peris and R. H. Crabtree, *Chem. Soc. Rev.*, 2018, **47**, 1959–1968.
47 Q. Yao, T. Chen, X. Yuan and J. Xie, *Acc. Chem. Res.*, 2018, **51**, 1338–1348.